2007 IEEE International Conference on
Robotics and Automation
Roma, Italy, 10-14 April 2007

On the Force Capabilities of Centripetal Force-actuated Microrobotic Platforms

P. Vartholomeos, *Student Member, IEEE,* K. Vlachos and E. Papadopoulos, *Senior Member, IEEE*

***Abstract*— In this paper a study is conducted on the force capabilities of centripetal force actuated microrobotic platforms. The aim is to exploit the centripetal forces generated by platform mounted vibrating micro-motors for micromanipulation purposes. First, an overview of the platform dynamics and motion capabilities is presented. The type of forces generated by the actuation mechanism as well as due to the impulsive interaction with the working environment are studied. Then design steps are proposed for (i) the reduction or elimination of undesired impulsive forces, (ii) the attenuation of the force ripple transmitted to the manipulated object. The outcome is a smooth, controllable force transmitted to the manipulated object. A cantilever is mounted on the platform and preliminary experiments are conducted.**

I. Introduction

In the last decade, micro-robotics has become an increasingly important field of research. Domains of application such as micro fabrication, biotechnology, microscopy and opto-electronics, demand miniaturized or micro-robotic platforms that provide ultra high precision, flexibility and a wide mobility range [1]. Furthermore, scientists that are involved in the emerging nano-technology will require a variety of novel tools to probe and manipulate their invisible specimens. To this end, extensive research has been carried out on the design and realization of both micro-manipulators and micro-robots. Motion principles and actuation mechanisms that combine sub-micrometer motion of high resolution and the speed virtues of coarse positioning have been the subject of intensive studies. Accurate manipulation of microspecimens not only requires sub-micrometric precision but also demands good understanding and control of the dynamics and the forces that are developed during manipulation. Therefore the study of the force capabilities of such microrobotic platforms and their manipulators is a very important part of the design and the implementation process [2,3].

Several micro-actuation techniques have been devised and are usually based on smart materials such as piezo-electric actuators, shape memory alloys, etc. The most popular micro-positioning motion mechanism is the stick-slip principle [4], which is implemented using piezoelectric actuators. This principle is employed by the MINIMAN micro-robot presented in [5]. These platforms are capable of positioning accuracy of less than 200*nm* and provide velocities of up to a few *mm/s*. The impact drive principle (a variant of stick-slip principle) is employed by the 3DOF micro-robotic platform Avalon, which provides step size of about 3.0 μm and speeds up to 1 *mm/s* and is presented in [6-7]. A different motion mechanism based on piezo-tubes is utilized by the Nano Walker micro-robot presented in [8]. The first prototypes of this micro-robot were capable for minimum steps of the order of 30 *nm* and demonstrated a maximum displacement rate of 200 *mm/s*. Possibly MiCRoN is the most advanced example of microrobotic platform, employing piezoelectric actuators, with integrated micromanipulator and is presented in [9-10].

Although piezoelectric actuators seem to be the favoured smart material for micro-positioning and do provide the required positioning resolution and actuation response, they usually suffer from complex power units that are expensive and cumbersome and which do not easily allow for untethered operation. In [11] the authors proposed a novel, simple and compact micro-robot that according to the theory in [12] is able to perform translational and rotational sliding with sub-micrometer positioning accuracy and velocities up to $1.5mm/s$. All the components of the mechanism including its driving units, are of low cost and readily available. The range of manipulation tasks of the platform presented in [12] involves several pushing operations such as positioning and aligning, with submicrometer precision, electro-optical miniature components whose weight ranges from a few milligrams to a few grams.

This paper presents results of the research carried out on the force capabilities of the microrobotic platform introduced in [12]. The contributions of this paper are: i) the analysis on the force capabilities of a platform actuated by vibration motors. ii) the derivation of design guidelines for the generation of smooth controllable forces, which can be used for micromanipulation tasks. iii) experimental validation of the theoretical results.

Paragraph II presents an overview of the platform dynamics and its motion capabilities. Paragraph III examines the type of forces generated due to the actuation mechanism as well as due to the impulsive interaction with the working

[1] This work is co-funded by the European Social Fund (75%) and National Resources (25%) - (EPEAEK II) – HRAKLEITOS.

P. Vartholomeos, K. Vlachos and E. Papadopoulos are with the Department of Mechanical Engineering, National Technical University of Athens, (NTUA) 15780 Athens (ph: +30-210-772-2643; fax: +30-210-772-1455; e-mail: barthol@central.ntua.gr).

environment. Design steps are proposed for (a) the reduction or elimination of undesired impulsive forces, (b) the attenuation of the force ripple transmitted to the manipulated object. Paragraph IV describes a preliminary experiment where the theoretical assertions are validated. The conclusions of this work are presented in paragraph V.

II. Platform Dynamics

Motion principle: The innovating actuation principle of the micro-robot is elaborated in [12]. What follows is a brief description of the physics that govern the motion principle. A simplified 1 dof mobile platform of mass M is used, whose motion mechanism employs an eccentric mass m, rotated by a platform mounted motor O, as shown in Fig. 1. One cycle of operation is completed when the mass has described an angle of 360°.

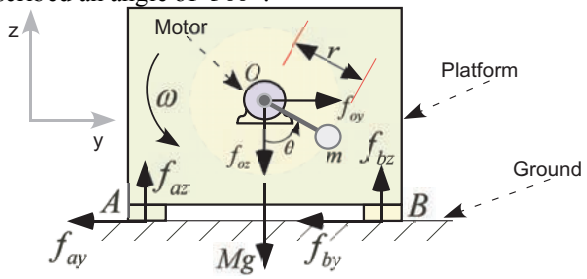

Fig. 1 Simplified 1dof platform with rotating mass m.

Gravitational and centripetal forces exerted on the rotating mass are resolved along the y-z axis to yield:

$$f_{oy} = mr\omega^2 \sin\theta$$
$$f_{oz} = -mg - mr\omega^2 \cos\theta \qquad (1)$$

where g is the acceleration of gravity and r the length of the link between m and O. Above a critical value of actuation speed $\omega_{critical}$ actuation forces overcome frictional forces and motion is induced. It has been shown analytically that the motion step the platform exhibits over a cycle can be made arbitrarily small depending on the actuation speed ω, [12]. Accordingly it has been demonstrated that the platforms motion resolution can be of submicrometer accuracy, [11,12]. Further reduction of resolution is hindered by the limited resolution of the electronics and by the non-uniform distribution of the surface coefficient of friction μ.

Platform dynamics: The actuation principle mentioned above was employed to the design of a 2dof micro-robot [11] as shown on figures 2a and 2b.

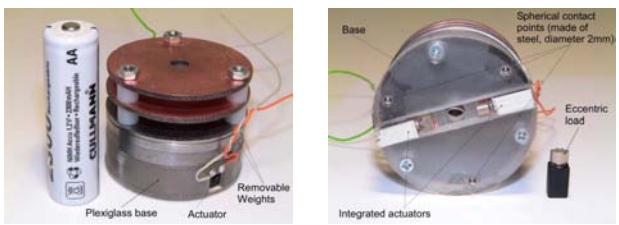

Fig 2. Platform: a. Lateral view b: Underside

The dynamics of the platform are provided in a compact matrix form by the usual Newton Euler equations [13]:

$$M\dot{\mathbf{v}} = \mathbf{R}\sum_i {}^b\mathbf{f}_i, \qquad i = \{a,b,c,d,e\} \qquad (2a)$$

$${}^b\mathbf{I}\dot{\boldsymbol{\omega}}_p + {}^b\boldsymbol{\omega}_p \times {}^b\mathbf{I}\,{}^b\boldsymbol{\omega}_p = \sum_i ({}^b\mathbf{r}_i \times {}^b\mathbf{f}_i) + \sum_i {}^b\mathbf{n}_j$$
$$i = \{a,b,c,d,e\},\ j = \{d,e\} \qquad (2b)$$

where $\mathbf{R}$ is a rotation matrix, $\boldsymbol{\omega}_p$ is the platform angular velocity, ${}^b\mathbf{I}$ is its inertia matrix, and $\mathbf{v} = [\dot{x}, \dot{y}, \dot{z}]^T$ is its center of mass (CM) position in the inertial frame. The subscripts $i = \{a,b,c\}$ correspond to frictional forces at the three contact points of the platform and $i = \{d,e\}$ corresponds to the two actuation forces generated by the two vibrating motors. During analysis equations are simplified due to planar motion

III. Generation of Manipulation Forces

In the previous paragraph the platform employed the centrifugal force actuation purely for accelerating itself in a controlled manner, i.e. for locomotion purposes. In this section it is demonstrated how these forces and the momentum acquired by the moving platform can be exploited for applying forces to microobjects. The primary goal is to generate controlled forces whose magnitude lies within the range of 50 to 500 mN and which can be used for primitive microassembly tasks such as pushing or aligning microobjects with sub-micrometric positioning accuracy. To this end a needle-type cantilever micromanipulator is mounted on the platform as shown in Fig 3a. Its diameter is 350μm, its length is 0.5cm and has a needle tip of 50 μm.

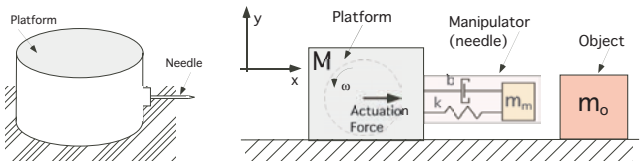

Fig. 3. a: Needle type cantilever b: Dynamic model

The generation of controlled manipulation forces poses a great challenge to the platform, which due to its driving principle, is constantly subjected to oscillating motion and to vibrating forces. First, the range and type of actuation forces is determined and second, the transmissibility characteristics of the platform-manipulator-object system are examined.

A. Force generation

An object that is been pushed by the platform is liable to experience two different type of forces: (i) the centrifugal actuation forces during contact and (ii) the impulsive forces due to successive impacts during the pushing operation.

Centrifugal actuation forces: The maximum centrifugal actuation forces that can be applied by the platform correspond to those forces that are exerted when the platform is blocked and produces zero motion. These are

called *blocking forces* and their maximum value has been analytically expressed as a function of actuation speed ω. These are plotted in Fig. 4a. It is also interesting to consider the max load mass that can be pushed by the platform as a function of actuation speed, ω. This relationship has been derived analytically -by considering the critical case where sliding of the platform and of the object is impeding and friction has reached its static limit- and is plotted in Fig. 4b

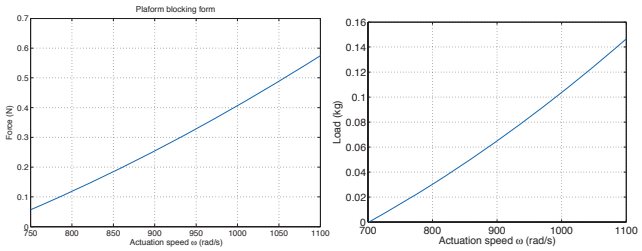

Fig. 4 Forces: a. Blocking b. Max load mass

In both graphs the upper bound actuation speed is imposed by the condition of static equilibrium along the vertical axis of the platform [12], i.e. greater actuation speeds result in tipping of the platform. The lower speed bound can be interpreted as the lowest actuation speed for which the centrifugal forces counteract the frictional forces and thus motion is induced. It is observed that the masses that can be conveyed by the platform are comparable to the mass of the platform.

Impulsive forces: The impulsive forces depend on the properties of the materials in contact. These affect the coefficient of restitution and also the relative velocity between the two bodies immediately before the impact. However the platform's approaching velocity right before the impact can have any random value in the feasible range of platform velocities, thus the amplitude of the corresponding impulsive forces is not easily predictable. It is useful though to have knowledge of the maximum impulse that an impact may exhibit as a function of the actuation speed ω and furthermore to simulate the impact and examine the response of the platform and of the object.

To this end the impact is modeled by the lumped parameter model depicted in Fig. 3b. The platform and the object are considered as rigid bodies having mass *M* and *m* respectively. For reasons of simplicity, it is assumed that the actuators are synchronized and thus no actuation moments are produced. Also it is assumed that the platform and the object are constrained to move along the x-axis only. At some instance, the platform may or may not be in contact with the object, in the latter case, the platform and the object behave as a single body. During contact the manipulator mass is incorporated into the object's mass and the dynamic equations are given in a compact state space form by:

$$\dot{\mathbf{x}} = \mathbf{A}\mathbf{x} + \mathbf{B}\mathbf{u} + \mathbf{G}f_{fr} \qquad (3)$$

where $x = [x_M, \dot{x}_M, x_m, \dot{x}_m]^T$, **A** is the system matrix containing mass-spring-damper constants, **B** and **G** are vectors that scale the input actuation force **u** (as given by Equ. 1) and the friction force f_{fr} described by the Coulomb model. Using numerical simulation of this model, the graph of maximum impulsive force versus actuation speed ω was generated and is presented in Fig. 5.

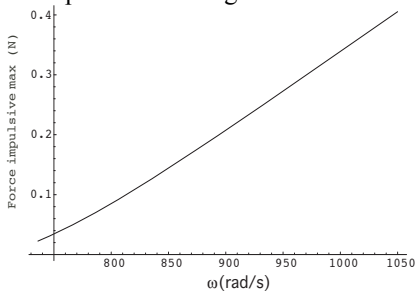

Fig. 5 Maximum impulsive forces

The dynamic behavior of the pushing operation is examined through numerical simulations using the physical parameters presented in Table 1. The displacements of the platform and of the object are depicted in Fig. 6.

TABLE 1

Parameter	Value	Parameter	Value
M	0.1 [kg]	k	$2.5 \cdot 10^6$ [N/m]
m	0.001 [kg]	b	200 [Ns/m]
μ	0.1	ω	800 [rad/s]

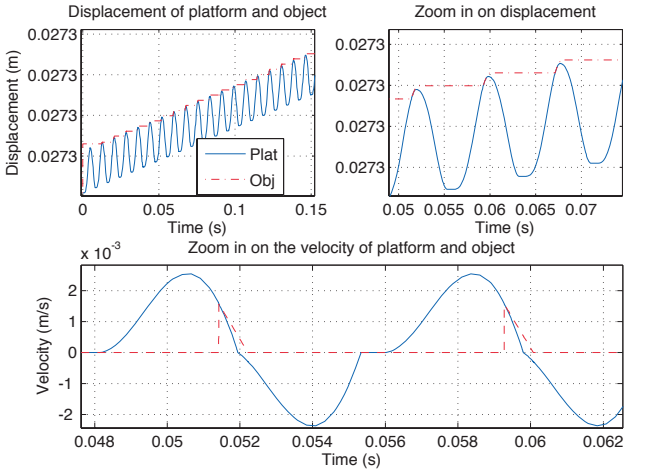

Fig. 6. Displacement and velocity of platform and object along x-axis.

In the first plot, the blue solid line represents the position of the point of contact on the manipulator tip and the red dashed line represents the position of the point of contact on the object. The platform initially is located at a distance of 5 μm away from the object and initially both platform and object are at rest. The third plot of Fig. 6 shows the velocities developed. It is observed that the object -whose mass is 100 times smaller than the platform's mass- develops instantaneously high velocity contrary to the platform whose velocity is slightly reduced. Figure 7 presents the forces applied to the object and to the manipulator.

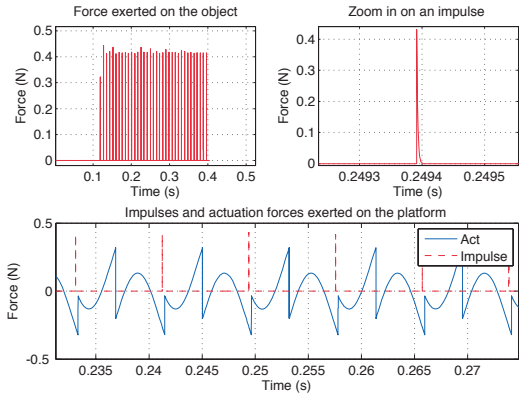

Fig. 7. Forces developed on the platform and the object.

The first plot demonstrates the impulse train that is applied to the object. As expected this train includes purely pushing forces only, i.e. the object cannot be pulled by the platform. The third plot of Fig. 7, demonstrates the forces that are experienced by the platform itself. Interestingly the force profile that the manipulator tip senses is richer than that of the object. This indicates that the platform and the object are in contact only during the impact period. In most applications actuation forces in the form of an impulse train are undesirable because the impulse magnitude is not predictable, it results in severe damage or wear of the pushed object and additionally gives rise to uncontrolled impulsive motion. Therefore it is of great importance to reduce or even eliminate the undesired impulsive behavior of the platform. This has been achieved through appropriate design of the manipulator system. The basic design steps and guidelines are presented in the next section.

B. *Impulse reduction and ripple attenuation.*

Impulse reduction: The ideal force generation is the one, where the platform smoothly pushes the object, remains attached to it, and no bouncing takes place. In this ideal case, the forces applied to the object are smooth and continuous, the manipulator is compressed by continuous compressive forces whose amplitude vary according to the centripetal actuation forces and the relative velocity of the two moving bodies. In that case no impulses appear and the object is subject to the forces that are transmitted through the manipulator. The model of Fig. 3b is used to study the impact reduction and to provide design guidelines for the manipulator. To simplify the calculations, it is assumed that the object remains static while been pushed by the manipulator, in this case the solution to Equ 3. is approximated by:

$$y(t) = A_o + B\cos(\omega t + \alpha) \qquad (4)$$

The variable $y(t)$ represents the displacement of the tip of the manipulator, which in this case is continuously in contact with the object. The solution describes a periodic forced response about a center of oscillation A_0. Should ω be large enough and k small enough, the manipulator is sufficiently compressed so that during oscillations its extension never exceeds its natural length. This is expressed mathematically by the following inequality:

$$A_0 + B \le l_0 \qquad (5)$$

where B is the oscillation's magnitude and l_0 is the manipulator's natural length. The useful ranges for ω and k were found by evaluating numerically the inequality (5). Fig. 8 presents the plot of the inequality's LHS versus k for $\omega = 900 rad/s$. In the following example l_0 is 15mm.

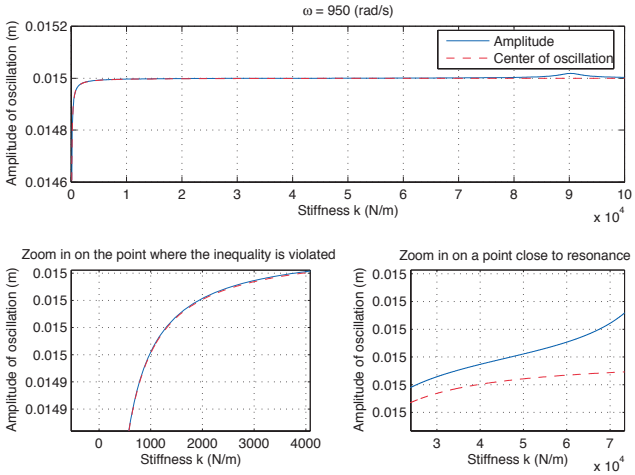

Fig. 8 Values lhs of inequality 4 as a function of k.

Hence, if during forced oscillations ω and k values lie within the range that satisfies the inequality, the manipulator remains compressed. Consequently the manipulator is not detached from the object and no impulses occur. The smooth peak the curve exhibits corresponds to the resonance frequency of the mass-spring-damper system. Simulation of the dynamic model using appropriate values for the design variable k and the control variable ω, verifies the assertion of the impulse elimination. Figure 9 depicts results of simulation of the displacement and force for values $\omega = 900 rad/s$, $k = 1 \cdot 10^3 \mathrm{N}/m$. The impulses have been eliminated, but the object is subject to forces with large ripple.

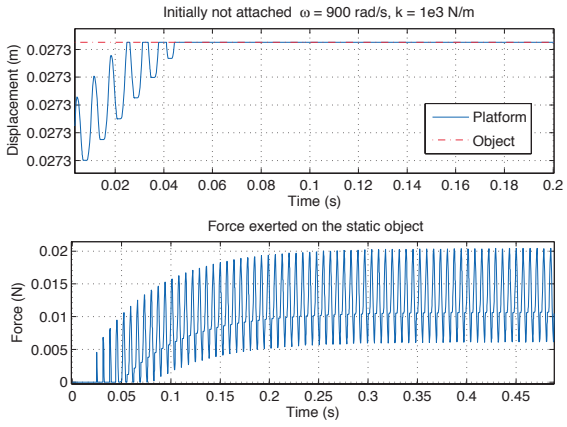

Fig. 9 Impulse elimination.

Force ripple attenuation: The next step is to reduce the ripple of the transmitted force. This means minimizing the magnitude of the actuation force F_m, which is expressed as:

$$F_m = f_k + f_b = ky(t) + b\dot{y}(t) \qquad (6)$$

The analytical expression of Equ. 6 is quite lengthy and is omitted from the present paper. The general guideline deduced from the analysis of Equ 6. suggests that for impulse elimination and for force ripple attenuation the values of k and b must be as small as possible. The factors that hinder the extreme reduction of these coefficients are: (i) practical considerations such the selection of appropriate materials for the construction of the manipulator system and (ii) the time constant of the manipulator system which increases as the k value reduces (parameter b cannot be very adjustable when pursuing a simple design). Figure 10 depicts forces developed for $k = 10^2$ and $b = 0.1$.

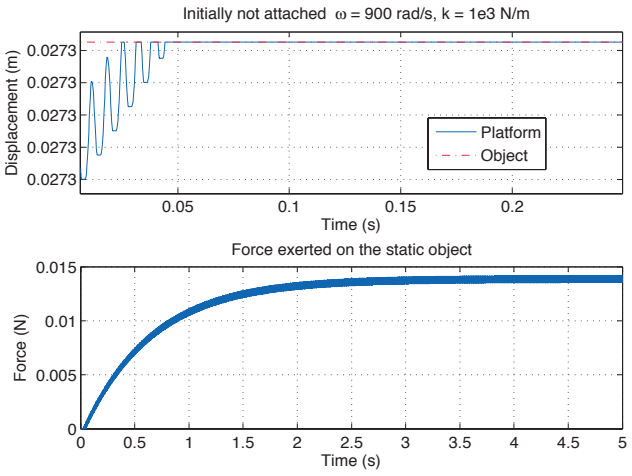

Fig. 10 Force ripple exerted on the object is suppressed.

The final selection of the k and b design values has led to a transmitted force that is impulse-free and with attenuated ripple. Furthermore the mean value of the steady state of this force response can be controlled by suitably adjusting the ω value. The above analysis was done for a static object. When the object is movable and is displaced by the manipulator during the pushing operation, the analysis becomes more complicated and analytical solutions cannot be derived. However numerical simulations indicate that although the impulses cannot be eliminated completely they can be substantially reduced following similar arguments with the simplified analysis presented above.

IV. Force Generation Experiments

Experiments were conducted in order to assess some of the results of the analysis and to examine and demonstrate the impulsive force transmission capabilities of the microrobotic platform. The experimental set-up is demonstrated in Fig. 11.

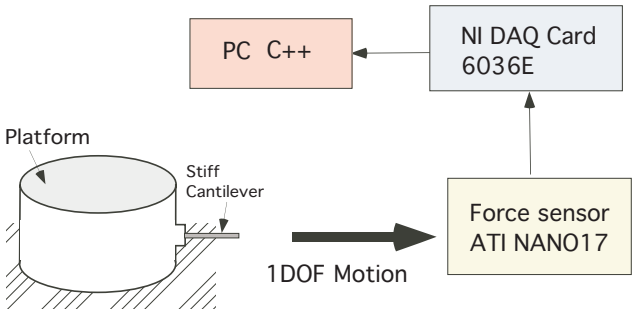

Fig. 11. Experimental set-up for 1DOF force measurement.

The force sensor remains static during the experiment. The microrobot is equipped with a high stiffness cantilever. Initially the microrobot was driven towards the force sensor at an actuation speed of $\omega_1 = 900 rad/s$. At approximately 2.5s the cantilever collided with the sensor and the exerted forces were measured. At approximately 6.5s the actuation speed reduced to $\omega_2 = 800 rad/s$. Fig. 12, plot a, presents the entire set of measurements made during the experiment. It is apparent that the force magnitude reduced as the actuation speed fell from 900 to 800 *rad/s*. Plot b depicts a zoom in on the measurements.

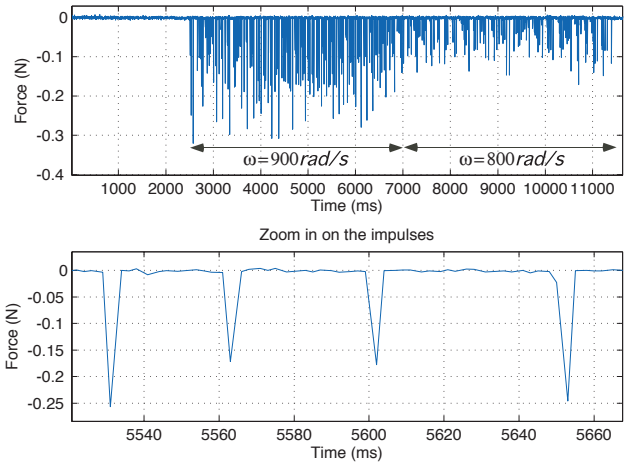

Fig. 12 Experimental measurements: Impulsive forces

As it was predicted by the analysis, the forces transmitted from the platform to the sensor through a stiff manipulator have impulse waveform. Their magnitude for 900rad/s is about 250 mN and for 800rad/s about 100mN. These experimental values are in accordance with what is presented in Fig. 5. The impulse frequency (as seen from Fig 12. Plot b) corresponds to about 1 to 3 cycles of actuation operation.

Finally a needle type cantilever was mounted on an aluminium base and was installed in the platform. Figure 13a illustrates the cantilever's tip as seen with an optical microscope. On the base of the cantilever a strain gauge was glued so as to measure the 1dof compressive forces the cantilever is subjected to (see Fig. 13b).

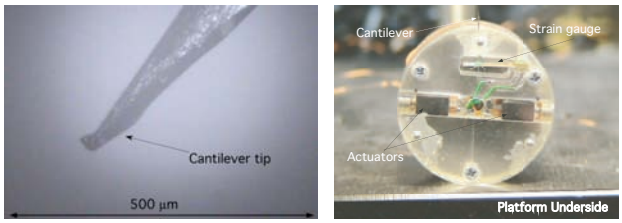

Fig. 13: Cantilever: a. Microscope view b. Strain gauge installation

The dimensions of the aluminum base were calculated so that the platform-needle system has stiffness less than $10^{-3} N/m$, i.e. sufficiently low so as to eliminate impulses. During the experiment, the microrobot was driven by an actuation speed of $920 rad/s$ towards a static object. At approximately 2.5s the cantilever tip reached the object. The forces transmitted by the needle were measured by the on-board strain gauge and are depicted on Fig 14a. Fig. 14b presents simulation results for the same set of parameters.

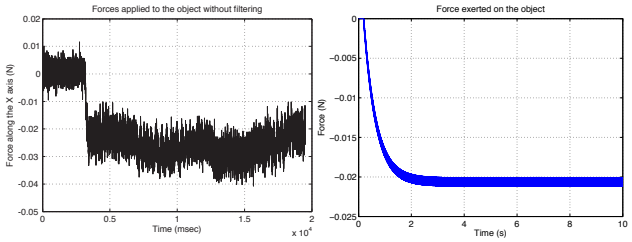

Fig. 14: a) Experimental measurement b) Simulation results.

Both graphs demonstrate that the impulsive forces have been eliminated. Comparing experimental and simulation results it is seen that the mean value of the force during simulation has an error of 17% with respect to the one during experimentation. This is owing to the non-modelled moments exerted on the needle by the platform and by the static object. Furthermore, simulations predict that the amplitude oscillation of the transmitted force should be reduced down to 5mN. However oscillations cannot be easily measured from the experimental data due to the electrical noise being present in the sensor electronics. The noise amplitude was measured during the first 2s of the experiment, where the needle was not yet in contact with the object, and was found to be equal to 10mN. During the rest of the experiment it is evident that the noise level is higher than that of the oscillations and no conclusions can be drown apart from the fact that oscillations peak-to-peak amplitude is less than 10mN

V. Conclusions

In this paper a study was carried out on the force capabilities of the microrobotic platform introduced in [12]. First, an overview of the platform dynamics and motion capabilities was presented. The type of forces generated by the actuation mechanism and by the impulsive interaction with the working environment were studied. Design steps were proposed for (i) the reduction or elimination of undesired impulsive forces, (ii) the attenuation of the force ripple transmitted to the manipulated object. A construction was realised where a high stiffness cantilever was mounted on the platform and experiments of impulsive motion were conducted. The magnitude and the frequency of the measured impulsive forces were in accordance with the simulation results. Next a needle-type cantilever was mounted on an aluminium sheet to form a low stiffness needle-platform system. Experiments conducted with this configuration demonstrated that the forces transmitted to the manipulated object were continuous, impulse-free and with reduced ripple. These results in combination with the microrobot's ultra-precise motion can be employed for pushing and accurately aligning very small parts.

References

[1] A. Kortschack, A. Shirinov, T. Truper, S. Faticow, "Development of Mobile Versatile Nanohandling Microrobots: Design, Driving Principles, Haptic Control," *Robotica, p. 419-434, July 2005*.

[2] A. Tafazzoli, C. Pawashe and M. Sitti, "Force controlled Microcontact Printing using Microassembled Particle Templates," *IEEE International Conference on Robotics and Automation (ICRA2006)*, Orlando, USA.

[3] Yu Sun, K. Kim, R.M. Voyles, B.J. Nelson, "Calibration of Multi-Axis MEMS Force Sensors Using the Shape from Motion," *IEEE International Conference on Robotics and Automation (ICRA2006)*, Orlando, USA.

[4] Jean-Marc Breguet, Reymond Clavel, "Stick and Slip Actuators: design, control, performances and applications," *International Symposium on Micromechatronics and Human Science (MHS)*, (Nagoya), 1998, 89-95.

[5] Schmoeckel, F., and Fatikow, S, "Smart Flexible Microrobots for Scanning Electron Microscope (SEM) Applications," *Journal of Intelligent Material Systems and Structures*, Vol. 11, No. 3, 2000, pp. 191-198.

[6] Büchi Roland, Zesch Wolfgang, Codourey Alain, "Inertial Drives for Micro- and Nanorobots: Analytical Study," *Proceedings of SPIE Photonics East '95: Proc. Microrobotics and Micromachanical Systems Symposium*, Vol. 2593, Philadelphia, PA, Lynne E. Parker - Bellingham, WA, SPIE, 1995

[7] Büchi Roland, Zesch Wolfgang, Codourey Alain, "Inertial Drives for Micro- and Nanorobots: Analytical Study," *Proceedings of SPIE Photonics East '95: Proc. Microrobotics and Micromachanical Systems Symposium*, Vol. 2593, Philadelphia, PA, Lynne E. Parker - Bellingham, WA, SPIE, 1995.

[8] Martel Sylvain et al., "Three-Legged Wireless Miniature Robots for Mass-scale Operations at the Sub-atomic Scale," *Proc. 2001 IEEE International Conference on Robotics & Automation*, Seoul, Korea, May 21-26, 2001, pp. 3423-3428.

[9] J. Brufau, M. Puig-Vidal, et. al, MICRON: Small Autonomous Robot for Cell Manipulation Applications, Proc. of the IEEE International Conference on Robotics & Automation, Barcelona, Spain, April 18-22, 2005.

[10] P. Vartholomeos, S. Loizou, M. Thiel, K. Kyriakopoulos and E. Papadopoulos, "Control of the Multi Agent Micro-Robotic Platform MiCRoN," IEEE International Conference on Control Applications, Munich, Germany, October 2006, (To Appear)

[11] P. Vartholomeos and E. Papadopoulos, "Analysis, Design and Control of a Planar Micro-robot Driven by Two Centripetal-Force Actuators," *IEEE International Conference on Robotics and Automation 2006 (ICRA2006)*, Orlando USA.

[12] P. Vartholomeos and E. Papadopoulos, "Dynamics, Design and Simulation of a Novel Microrobotic Platform Employing Vibration Microactuators," Journal of Dynamic Systems, Measurement and Control, ASME, March 2006.

[13] L. Sciavicco and B. Siciliano, "Modelling and Control of Robot Manipulators," Springer 2003.